

**Quantum interference and exceptional points in a nonreciprocal two-level system**Jing Dong <sup>1</sup>, Xiao-Lin Li,<sup>2</sup> Fu-Quan Dou,<sup>1</sup> and Wen-Yuan Wang <sup>1,\*</sup><sup>1</sup>*College of Physics and Electronic Engineering, Northwest Normal University, Lanzhou 730070, China*<sup>2</sup>*School of Physics, Northwest University, Xi'an 710127, China* (Received 3 August 2023; revised 30 October 2023; accepted 22 November 2023; published 8 December 2023)

Non-Hermitian systems with complex-valued energy spectra and exceptional points show unconventional dynamics. Here we investigate the quantum interference of a self-interacting two-level system in which the coupling between the levels is nonreciprocal. We propose the multiple-passage Landau-Zener-Stückelberg-Majorana scheme to realize the quantum interferometry of such a non-Hermitian system, that is, the energy bias between two levels is periodically modulated, which may result in constructive or destructive interference. In the absence of nonlinear self-interaction, it exhibits obvious interference fringes in the weak nonreciprocal regime, whereas the interference is completely suppressed in the strong nonreciprocal regime due to the parity-time-symmetry breaking. The explicit expressions for the occupation probabilities are obtained within an effective rotating-wave approximation, which is consistent with the numerical results. In the presence of nonlinear interaction, the system shows a rich variety of dynamics and interference fringes. We further obtain phase diagrams for large ranges of nonreciprocity and nonlinear interaction parameters to explicitly demonstrate quantum interference within the nonlinear non-Hermitian system. The present work unlocks quantum interference characteristics from a nonreciprocal two-level system and provides a theoretical perspective for the manipulation of quantum states in non-Hermitian systems.

DOI: [10.1103/PhysRevA.108.063506](https://doi.org/10.1103/PhysRevA.108.063506)**I. INTRODUCTION**

Quantum interference is the underlying principle of quantum information processing protocols. The model of a quantum two-level system (TLS) is a paradigm for investigating a variety of quantum dynamics phenomena. Among them, Landau-Zener tunneling is a well-known dynamical phenomenon that describes quantum transitions between the two energy levels of a two-level system traversing the avoided-crossing region [1,2]. When the control parameter is varied periodically, such that the TLS keeps going back and forth across the avoided-crossing region, a sequence of consecutive Landau-Zener tunneling events leads to a periodic dependence on the occupation probabilities of the two levels [3,4]. This phenomenon is often referred to as Landau-Zener-Stückelberg-Majorana (LZSM) quantum interference [5–7]. In the past few decades, LZSM interference has been experimentally observed in a number of physical systems such as ultracold molecular gases [8], optical lattices [9], nitrogen-vacancy centers in diamond [10–12], and spatial LZSM interference [13].

In the present paper we investigate quantum interference in a non-Hermitian TLS, in which the non-Hermiticity is induced by the nonreciprocal coupling between the levels. Non-Hermitian Hamiltonian systems often appear as an effective description of phenomena which are associated with nonconservative systems of various forms [14–23], especially in the context of parity-time ( $\mathcal{PT}$ )-symmetric systems [14,24–

26]. In recent years, there have been remarkable developments in the use of non-Hermitian Hamiltonians in the study of open quantum systems [14–22]. Furthermore, non-Hermitian systems with gain and loss [17,27–32] can also be mapped onto nonreciprocal systems. When a quantum system couples to a surrounding environment or bath, the dynamics of the system itself becomes non-Hermitian and features quantum transitions [18], i.e., the nonreciprocity of state transitions, and it can be utilized to engineer an effective non-Hermitian Hamiltonian [20,21,31,33] that preserves the time-reversal symmetry while breaking the parity symmetry, so asymmetric transport is expected to arise. The Bogoliubov–de Gennes equation, which characterizes the dynamics of noncondensed atoms in a Bose-Einstein condensate [34–36], possesses this type of symmetry. The non-Hermitian Su-Schrieffer-Heeger model with asymmetric intra-unit-cell hopping amplitudes has been realized by this approach [37]. Nonreciprocity exists in various physical contexts and finds applications in topological photonics [38,39], nonlinear metamaterials [40,41], and optical communication and information processing [42–45]. Recently, tunable nonreciprocal hopping was implemented in the quantum trajectory approach [46–50] and realized in recent experiments with single photons [51] and ultracold atoms [20,52–57].

Non-Hermitian generalizations of the LZSM model have been presented, including the pseudo-Hermitian LZSM model [58], the nonlinear non-Hermitian TLS [59], and LZSM interferometry in  $\mathcal{PT}$ -symmetric optical waveguides [60]. In addition, the captivating physical phenomena that arise from the interplay between non-Hermitian and nonlinear effects have garnered significant attention from researchers [18]. For

\*wywang@nwnu.edu.cn

example, nonlinearity can transform the system from broken to full  $\mathcal{PT}$  symmetry [61]. Nonlinear  $\mathcal{PT}$ -symmetric optical coupled systems can be realistically synthesized on semiconductor wafers [62,63]. All-dielectric unidirectional devices have been demonstrated by exploiting the interplay between non-Hermiticity and nonlinearity [64,65]. The non-Hermitian quantum dynamics differs drastically from its unitary counterpart, and its generic features are far from being fully understood. In particular, the investigation of the quantum interference and exceptional points (EPs) for non-Hermitian systems is only at its beginning [66,67].

In this paper we study the quantum interference of a non-Hermitian system with multiple-passage LZSM interferometry in a nonreciprocal TLS, focusing on the impact of EPs on quantum interference, especially in the presence of nonlinear self-interaction. In the absence of the nonlinear self-interaction, the appearance of EPs significantly changes the dynamical behavior of the system, leading to the breakdown of quantum interference. A suitable rotating-wave approximation (RWA) is used to obtain a good description of the dynamics. In the presence of nonlinear interaction, the system exhibits a rich variety of dynamics and interference fringes originating from the competition between the nonreciprocity and nonlinear interaction.

The rest of the paper is organized as follows. We first construct quantum interference of a non-Hermitian system with LZSM interferometry in a nonreciprocal TLS in Sec. II. Then we study quantum interference in the absence of the nonlinear self-interaction in Sec. III, focusing on the impact of EPs on quantum interference. In Sec. IV we study the nonreciprocal LZSM interference in the presence of nonlinear interactions. A summary is presented in Sec. V.

## II. SCHEME OF QUANTUM INTERFERENCE IN A NONRECIPROCAL TWO-LEVEL SYSTEM

We consider a nonreciprocal TLS in which the dynamics is governed by the dimensionless Schrödinger equation [22]

$$i \frac{d}{dt} \begin{pmatrix} a \\ b \end{pmatrix} = \begin{pmatrix} \frac{\gamma}{2} + c|a|^2 & \frac{\nu}{2} \\ \frac{\nu}{2}(1 - \delta) & -\frac{\gamma}{2} + c|b|^2 \end{pmatrix} \begin{pmatrix} a \\ b \end{pmatrix}, \quad (1)$$

where  $(a, b)$  is the two-mode wave function,  $\nu$  is the coupling strength between the two levels,  $\delta$  denotes the nonreciprocity parameter which introduces asymmetry in the system and leads to non-Hermiticity,  $\gamma$  is the level bias, and  $c$  represents the nonlinear self-interaction parameter which indicates the population-dependent level energy. Furthermore,  $c$  represents the nonlinear parameter signifying the interaction strength among atoms, with  $c > 0$  indicating repulsive interaction. Since the Hamiltonian can be scaled by dividing by  $\nu$ , for convenience, we can set  $\nu = 1$  as the energy unit hereafter.

To construct quantum interference of a non-Hermitian system with multiple-passage LZSM interferometry in such a self-interacting nonreciprocal TLS, we assume the energy bias between two levels is periodically modulated as

$$\gamma(t) = A \cos(\omega t), \quad (2)$$

where  $A$  and  $\omega$  are the amplitude and frequency of the driving field, respectively. When the control parameter  $\gamma(t)$  is varied

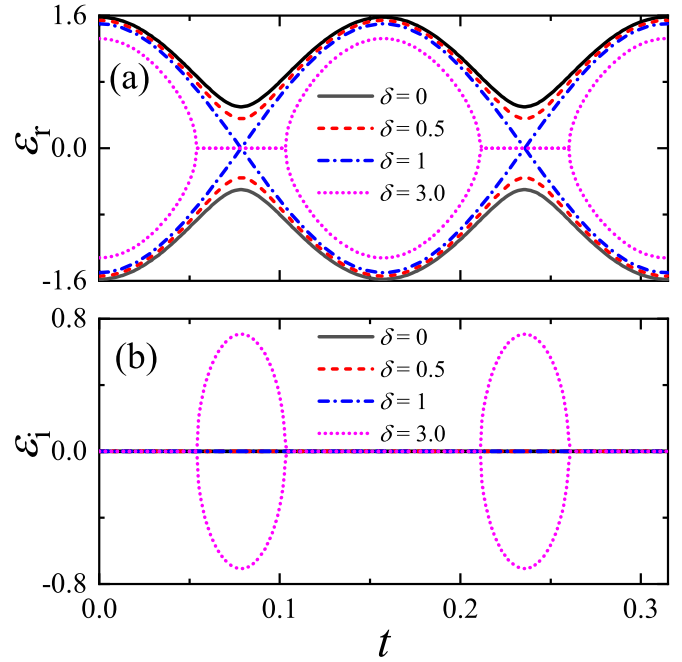


FIG. 1. Time evolution of the energy levels during one period in the absence of the nonlinear self-interaction (i.e.,  $c = 0$ ): (a) real and (b) imaginary parts of the energy levels. For  $\delta \leq 1$ , the imaginary parts of energy are always 0, and they overlap in (b). For  $\delta > 1$ , i.e.,  $\delta = 3$ , a series of EPs have appeared. The amplitude and frequency of the modulation field are  $A = 3$  and  $\omega = 20$ , respectively.

periodically such that the system keeps going back and forth across the avoided-crossing region (or the EPs in the strong nonreciprocity regime), a sequence of consecutive Landau-Zener tunneling events leads to periodic dependence on occupation probabilities of the two levels, namely, multiple-passage LZSM interferometry. In the present paper we focus on the high-frequency driving case, i.e.,  $\omega \gg \nu$ .

In the absence of the nonlinear self-interaction (i.e.,  $c = 0$ ), the energy levels of the system depend on the level bias  $\gamma(t)$  as follows:

$$\varepsilon_{\pm}(t) = \pm \frac{1}{2} \sqrt{\gamma^2(t) + \nu^2(1 - \delta)}. \quad (3)$$

Obviously, when  $\gamma^2(t) + \nu^2(1 - \delta) < 0$ , the system allows imaginary energy levels to exist, i.e.,  $\varepsilon = \varepsilon_r + i\varepsilon_i$ , with  $\varepsilon_r$  and  $\varepsilon_i$  the real and imaginary parts of energy, respectively. Figure 1 shows the energy spectrum of a non-Hermitian model plotted against time, which describes a full cycle of the LZSM interference [6]. When  $\delta < 1$ , the real parts of eigenvalues present many periodic avoided level crossings, and the imaginary parts of the eigenvalues remain constant at zero. This scenario gives rise to the phenomenon of LZSM interference within the system. However, avoided level crossings disappear and the upper and lower energy levels cross at  $t = \frac{(2k+1)\pi}{2\omega}$  ( $k \in \mathbb{Z}$ ) for  $\delta = 1$ . For  $\delta > 1$ , the real parts of the eigenvalues coalesce and become zero between two EPs at which two eigenvalues and their corresponding eigenvectors coalesce, while the corresponding imaginary parts of the eigenvalues are nonzero. Obviously, the nonreciprocity parameter  $\delta$  greatly affects the level structure of the system. Therefore, we are also interested in investigating the influence of the nonreciprocity parameter

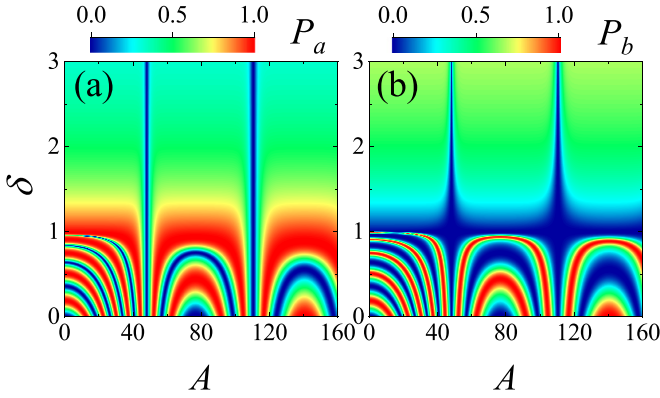


FIG. 2. Nonreciprocal quantum interference patterns in the absence of the nonlinear self-interaction (i.e.,  $c = 0$ ). Level occupation probabilities (a)  $P_a$  and (b)  $P_b$  for the system are initially found in the upper and lower energy levels, respectively. Here the quantum interference patterns are obtained by recording the final occupancy probability  $P_a$  (or  $P_b$ ) during 100 periods of the LZSM process, i.e.,  $t = 10\pi$  for  $\omega = 20$ .

on the dynamic evolution of the occupation probability under different initial conditions.

The nonlinear Schrödinger equation (1) of the nonreciprocal TLS can be solved numerically using standard Runge-Kutta fourth- and fifth-order algorithms. In order to study the characteristics of nonreciprocal quantum interference, we assume that the system is initially found in the lower (upper) energy level, i.e.,  $(a(t=0), b(t=0))^T = (1, 0)^T$  [ $(a(t=0), b(t=0))^T = (0, 1)^T$ ]. Since the TLS is non-Hermitian, the time evolution is no longer unitary and the total population, i.e.,  $N(t) = |a(t)|^2 + |b(t)|^2$ , is not a conserved quantity. Thus, the occupancy probability of each energy level can be defined as

$$P_a \equiv \frac{|a(t)|^2}{N(t)}, \quad P_b \equiv \frac{|b(t)|^2}{N(t)}. \quad (4)$$

Then the quantum interference fringe patterns can be obtained by recording the occupancy probability  $P_a$  ( $P_b$ ) for the system, which is initially found in the upper (lower) energy level, i.e.,  $(a(t=0), b(t=0))^T = (0, 1)^T$  [ $(a(t=0), b(t=0))^T = (1, 0)^T$ ].

### III. QUANTUM INTERFERENCE IN THE ABSENCE OF NONLINEAR SELF-INTERACTION ( $c = 0$ )

#### A. Breakdown of quantum interference by strong nonreciprocity

Let us now study quantum interference with the multiple-passage LZSM process, where the system passes the avoided-crossing region (or EPs) periodically. We begin our numerical simulations of quantum interference in the absence of the nonlinear self-interaction (i.e.,  $c = 0$ ) during 100 periods, i.e.,  $t = 10\pi$ . Figures 2(a) and 2(b) depict quantum interference patterns as a function of the nonreciprocity parameter  $\delta$  and the driving amplitude  $A$  for the system that is initially found in the upper and lower energy levels, respectively.

In the weak nonreciprocal regime (i.e.,  $\delta < 1$ ), conspicuous interference fringes are discernible, whereas the interference

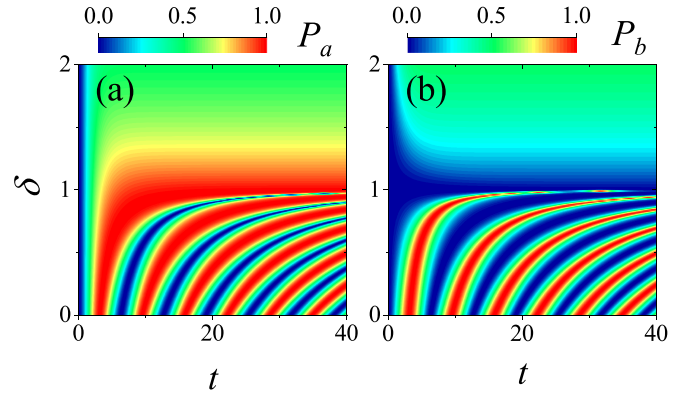


FIG. 3. Nonreciprocal time-domain interference patterns of the multiple-passage LZSM process for the nonreciprocity parameter  $\delta$  ranging from 0 to 2. Occupation probabilities (a)  $P_a$  and (b)  $P_b$  are shown as a function of time, assuming that the system was initially found in the upper and lower energy levels, respectively. Here the driving frequency  $\omega = 20$  and driving amplitude  $A = 3$ .

is completely suppressed in the strong nonreciprocal regime (i.e.,  $\delta > 1$ ) due to the  $\mathcal{PT}$ -symmetry breaking. Meanwhile, the interference fringes observed in Figs. 2(a) and 2(b) exhibit obvious differences, indicating a clear nonreciprocal quantum interference. In the absence of a nonreciprocity parameter (i.e.,  $\delta = 0$ ), the quantum interference fringe patterns of  $P_a$  are the same as those of  $P_b$ , which corresponds to the Hermitian case. In the weak nonreciprocal regime, as the nonreciprocal parameter  $\delta$  increases, the difference in interference fringes becomes increasingly apparent. We also notice that at certain amplitudes, regardless of the strength of nonreciprocity, the occupation probabilities  $P_a$  and  $P_b$  are always zero, namely, at certain combinations of the driving parameters, the tunnelings between two levels are frozen, which is the so-called coherent destruction of tunneling (CDT) [68].

#### B. Nonreciprocal time-domain interference patterns and theoretical analysis

In this section we present the numerical results and compare them with the theoretical predictions to gain a deeper understanding of non-Hermitian quantum interference patterns. In Figs. 3(a) and 3(b) we present the numerical results for the nonreciprocal time-domain interference patterns obtained with the multiple-passage LZSM process for the nonreciprocity parameter  $\delta$  ranging from 0 to 2. Figure 3(a) shows the occupation probabilities  $P_a$ , assuming that the system was initially found in the upper energy levels, i.e.,  $(a(t=0), b(t=0))^T = (0, 1)^T$ . Figure 3(b) shows the occupation probabilities  $P_b$ , assuming that the system was initially found in the lower energy levels, i.e.,  $(a(t=0), b(t=0))^T = (1, 0)^T$ . Here the driving frequency and driving amplitude are  $\omega = 20$  and  $A = 3$ , respectively.

Obviously, in the absence of nonreciprocity, that is, when the system degenerates into the Hermitian case, the numerical results of the time-domain interference patterns  $P_a$  and  $P_b$  in Figs. 3(a) and 3(b) obtained with the multiple-passage LZSM process are completely consistent. As the nonreciprocal parameter increases, the difference in interference fringes

between  $P_a$  and  $P_b$  becomes increasingly significant. Nevertheless, the observation manifests as conspicuous interference fringes in the weak nonreciprocal regime, i.e.,  $\delta < 1$ . Conversely, in the regime of strong nonreciprocity, i.e.,  $\delta > 1$ , the time-domain interference is completely suppressed. In this regime, both  $P_a$  and  $P_b$  start from 0 and monotonically increase towards certain values with periodic modulation. Through numerical observations, we find through enough LZSM processes that the values depend solely on the nonreciprocity parameter in the forms of  $P_a = 1/\delta$  and  $P_b = (\delta - 1)/\delta$ , as shown in Figs. 3(a) and 3(b).

Now we explain the above numerical results through some analytic deduction. Considering that the frequency of the driving field is large enough in the present paper, namely, the high-frequency driving case, i.e.,  $\omega \gg \nu$ , we can use the RWA to analyze the above interesting phenomenon [68–70]. After a series of careful deductions, we finally obtain the analytic expressions of  $P_a$  and  $P_b$  (details can be found in Appendix A). For the system initially found in the upper energy level, i.e.,  $(a(t=0), b(t=0))^T = (0, 1)^T$ , we have

$$P_a = \frac{1}{\delta + (1 - \delta) \operatorname{csc}^2(B\sqrt{1 - \delta}t)} \quad (\delta < 1), \quad (5a)$$

$$P_a = \frac{1}{\delta + (\delta - 1) \operatorname{csch}^2(B\sqrt{\delta - 1}t)} \quad (\delta > 1). \quad (5b)$$

Here  $B = \frac{\nu}{2} J_0(A/\omega)$  and  $J_0(A/\omega)$  is the zeroth-order Bessel function of the first kind. For the system initially found in the lower energy level, i.e.,  $(a(t=0), b(t=0))^T = (1, 0)^T$ , we have

$$P_b = \frac{\delta - 1}{\delta} \left( 1 - \frac{2}{2 - \delta + \delta \cos(2B\sqrt{1 - \delta}t)} \right) \quad (\delta < 1), \quad (6a)$$

$$P_b = \frac{\delta - 1}{\delta} \left( 1 - \frac{2}{2 - \delta + \delta \cosh(2B\sqrt{\delta - 1}t)} \right) \quad (\delta > 1). \quad (6b)$$

In Fig. 4 we present the nonreciprocal time-domain interference patterns of multiple-passage LZSM processes  $P_a$  and  $P_b$  obtained by directly integrating the time-dependent nonlinear Schrödinger equation and compare them with the above analytical formula calculated from the RWA. Interestingly, we find that they match each other well both in the weak nonreciprocal regime ( $\delta < 1$ ) and in the strong nonreciprocal regime ( $\delta > 1$ ).

The theoretical results of the expressions (5) and (6) can well explain the patterns of constructive and destructive interference in the weak nonreciprocal regime and can also explain the phenomenon that the quantum interference can be completely suppressed in the strong nonreciprocal regime. In the weak nonreciprocal regime, from Eqs. (5a) and (6a) we readily obtain that the constructive interference occurs at  $t = \frac{(2n+1)\pi}{\sqrt{1-\delta}\nu|J_0(\frac{A}{\omega})|}$ ,  $n \in \mathbb{Z}$ , whereas the destructive interference occurs at  $t = \frac{2n\pi}{\sqrt{1-\delta}\nu|J_0(\frac{A}{\omega})|}$ ,  $n \in \mathbb{Z}$ . We can also obtain the distances of interference fringes as  $\Delta = \frac{2\pi}{\sqrt{1-\delta}\nu|J_0(\frac{A}{\omega})|}$ . In the strong nonreciprocal regime, from Eqs. (5b) and (6b) we can obtain that through enough LZSM processes, the values depend solely on the nonreciprocity parameter in the forms of

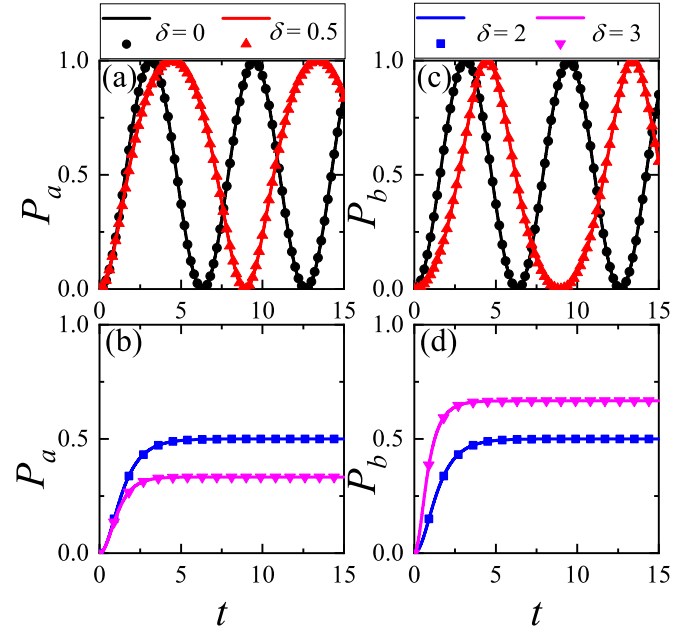


FIG. 4. Comparison of the nonreciprocal time-domain interference patterns of the multiple-passage LZSM process (a) and (b)  $P_a$  and (c) and (d)  $P_b$  obtained by directly integrating the time-dependent nonlinear Schrödinger equation (circles) and the theoretical results obtained using the expressions (5) and (6) (solid lines) for (a) and (c) the weak nonreciprocal regime, i.e.,  $\delta < 1$ , and (b) and (d) the strong nonreciprocal regime, i.e.,  $\delta > 1$ .

$P_a = 1/\delta$  and  $P_b = (\delta - 1)/\delta$ , which are consistent with the numerical observations shown in Figs. 3(a) and 3(b).

### C. Theoretical analysis of the CDT phenomenon on interference patterns

Figures 2(a) and 2(b) illustrate the CDT phenomenon on interference patterns, namely, for certain combinations of the driving parameters, the tunneling between two levels is frozen. In this section we provide a theoretical analysis of the CDT phenomenon by utilizing the theory presented under the RWA. In Fig. 5 we show nonreciprocal time-domain interference patterns of the multiple-passage LZSM process for large ranges of driving amplitude  $A$ . A notable feature is that there are obvious differences between  $P_a$  and  $P_b$ , which can be attributed to the presence of nonreciprocity. Figures 5(a) and 5(c) represent  $P_a$  for  $\delta = 0.5$  and 3, respectively. Figures 5(b) and 5(d) represent  $P_b$  for  $\delta = 0.5$  and 3, respectively. Interestingly, we find that in both the weak nonreciprocal regime and the strong nonreciprocal regime, the CDT occurs. In the weak nonreciprocal regime, except for the specific amplitudes at which CDT occurs, the system always exhibits significant time-domain interference behavior for other driving amplitudes. In contrast, in the strong nonreciprocal regime, regardless of the magnitude of the driving amplitude, the system does not exhibit time-domain interference behavior. This is consistent with the theoretical results predicted by the RWA for the expressions (5) and (6). Therefore, this agreement between the theoretical and numerical values further

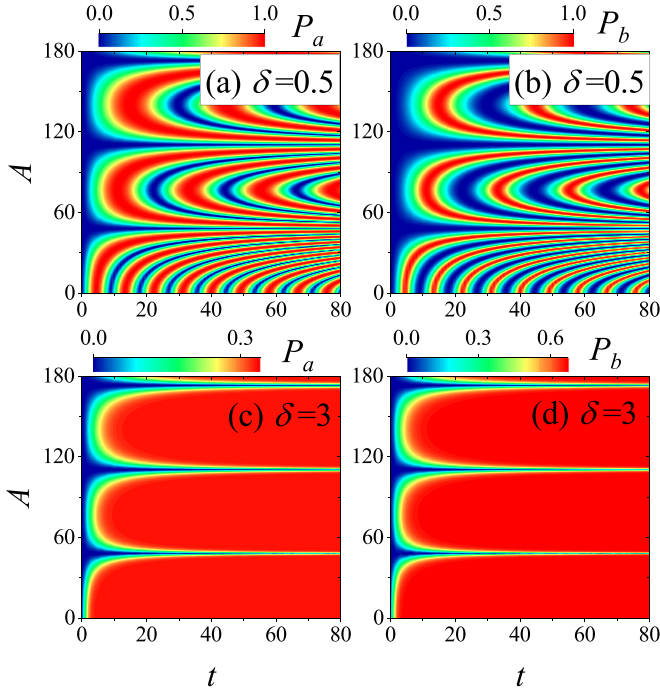


FIG. 5. Nonreciprocal time-domain interference patterns of the multiple-passage LZSM process for large ranges of driving amplitude  $A$ :  $P_a$  for (a)  $\delta = 0.5$  and (c)  $\delta = 3$  and  $P_b$  for (b)  $\delta = 0.5$  and (d)  $\delta = 3$ . The CDT occurs in both (a) and (b) weak and (c) and (d) strong nonreciprocal regimes.

confirms the validity of the RWA in predicting the behavior of interference.

The numerical observation of CDT can be explained using the above approach [68–70]. Within the framework of the RWA and considering the high-frequency approximation that the present paper focuses on, we can readily obtain that the condition of CDT occurs from the reduced Hamiltonian (A7) in Appendix A, that is,

$$J_0\left(\frac{A}{w}\right) = 0. \quad (7)$$

Therefore, the frequency of oscillations vanishes and the oscillations are consequently suppressed when the parameters satisfy the above CDT condition (7). The above predictions are completely consistent with our numerical observations.

#### IV. QUANTUM INTERFERENCE OF THE NONRECIPROCAL TLS IN THE PRESENCE OF NONLINEAR INTERACTION ( $c \neq 0$ )

Now we focus on the effect of nonlinear interactions on the quantum interference of a nonreciprocal TLS. In the presence of atomic interaction, even in the high-frequency driving case under the framework of the RWA, the system (1) is no longer analytically solvable. It is found that the dynamics of a TLS can be strongly modified by the nonlinear interaction [71–79]. Our numerical simulations for the effects of nonlinear interaction  $c$  and the driving amplitude  $A$  on the nonreciprocal quantum interference patterns are displayed in Fig. 6, in which the quantum interference patterns are obtained by recording

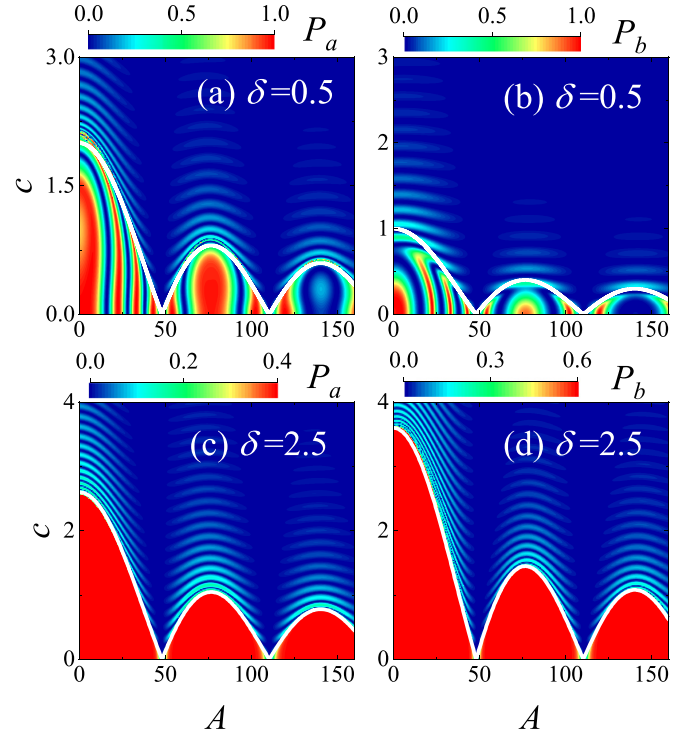


FIG. 6. Nonreciprocal quantum interference patterns in the presence of the nonlinear self-interaction. (a) and (b) Weak nonreciprocal regime, i.e.,  $\delta = 0.5$ . In both (a) and (b), a white solid line divides the phase plane into two parts: The region above the line is the self-trapping phase and the region below the line is the quantum interference is maintained phase. (c) and (d) Strong nonreciprocal regime, i.e.,  $\delta = 2.5$ . In both (c) and (d), a white solid line divides the phase plane into two parts: The region above the line is the self-trapping phase and the region below the line is the phase in which quantum interference is broken down by a strong nonreciprocity. Here the quantum interference patterns are obtained by recording the final occupancy probability  $P_a$  (or  $P_b$ ) during 100 periods of the LZSM process, i.e.,  $t = 10\pi$  for  $\omega = 20$ .

the final occupancy probability  $P_a$  (or  $P_b$ ) during 100 periods of the LZSM process, i.e.,  $t = 10\pi$  for  $\omega = 20$ . Figures 6(a) and 6(c) present  $P_a$  for the system initially found in the upper energy levels. Figures 6(b) and 6(d) present  $P_b$  for the system initially found in the lower energy levels.

Figures 6(a) and 6(b) depict the nonreciprocal quantum interference patterns of the multiple-passage LZSM process in the weak nonreciprocal regime, i.e., we take  $\delta = 0.5$  as an example. Two regions are observed, which are separated by a white solid line. The region above the line corresponds to the self-trapping phase, in which the strong nonlinear interaction  $c$  blocks the Josephson oscillation of the particle between the two energy levels, characterized by a nonzero temporal mean of the population imbalance [71–74,76]. The region below the line shows the phase in which quantum interference is maintained, in which the interference fringes are modulated by both the nonlinear interaction parameter  $c$  and the driving amplitude  $A$ . In Fig. 6(a) the region where quantum interference is maintained is approximately within the parameter range  $c < f(\delta)|J_0(A/\omega)|$ . In Fig. 6(b) the region in which

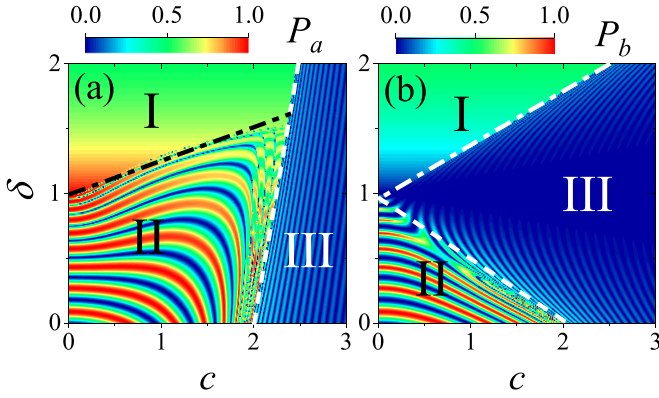


FIG. 7. Phase diagram of the nonreciprocal quantum interference patterns in the parameter plane  $(c, \delta)$ : (a)  $P_a$  and (b)  $P_b$ . There are three regions. Region I is the phase in which quantum interference is broken down by a strong nonreciprocity. Region II is the phase in which quantum interference is maintained. Region III is the self-trapping phase. Here the quantum interference patterns are obtained by recording the final occupancy probability  $P_a$  (or  $P_b$ ) during 100 periods of the LZSM process, i.e.,  $t = 10\pi$  for  $\omega = 20$  and  $A = 3$ .

quantum interference is maintained can be approximated by the parameter range  $c < f_1(\delta)|J_0(A/\omega)|$ .

For the strong nonreciprocal regime, the phase diagrams of nonreciprocal quantum interference patterns are shown in Figs. 6(c) and 6(d) for  $\delta = 2.5$ . A white solid line divides the phase diagram into two parts. The region above the line corresponds to the self-trapping phase and the region below the line represents the phase in which quantum interference is broken down by the strong nonreciprocity phase. We find that, interestingly, in the phase in which quantum interference is broken down by strong nonreciprocity, our calculations indicate that the nonlinear interaction effects can be completely suppressed so that the  $P_a$  and  $P_b$  are identical to their linear counterparts in Eqs. (5b) and (6b), respectively. Figures 6(c) and 6(d) show the regions where quantum interference is broken down by a strong nonreciprocity approximately within parameter range  $c < f_2(\delta)|J_0(A/\omega)|$ .

To gain further insight into the effects of the nonlinear interaction  $c$  and nonreciprocity parameter  $\delta$  on quantum interference, we present the phase diagram of quantum interference for a large range of nonreciprocity and nonlinearity parameters in Fig. 7, which shows the nonreciprocal quantum interference patterns characterized by  $P_a$  [Fig. 7(a)] and  $P_b$  [Fig. 7(b)] during 100 periods of the LZSM process, i.e.,  $t = 10\pi$  for  $\omega = 20$  and  $A = 3$ . There are three regions in both Figs. 7(a) and 7(b). Region I is the phase in which quantum interference is broken down by a strong nonreciprocity, where the nonlinear interaction effect is completely suppressed by the strong non-Hermiticity so that  $P_a$  and  $P_b$  are only dependent on the nonreciprocal parameter  $\delta$ . Region II shows the phase in which the quantum interference is maintained, where the nonlinear interaction  $c$  and the nonreciprocity parameter  $\delta$  can jointly modulate quantum interference fringes. Region III is the self-trapping phase. In Fig. 7(a), one phase-change line (dash-dotted line) is estimated as  $\delta = 1 + g_1(A)c$ , while another phase-change line (dashed line) is estimated as  $\delta =$

$g_2(A)(1 - 0.5c)$ . In Fig. 7(b), one phase-change line (dash-dotted line) is estimated as  $\delta = 1 + g_3(A)c$ , while another phase-change line (dashed line) is estimated as  $\delta = 1 - 0.5c$ .

## V. CONCLUSION

In this paper we explored the dynamics of a TLS in which the non-Hermitian effects are introduced by making the hopping between the levels nonreciprocal [22]. Recently, there has been significant progress in realizing such tunable nonreciprocal hopping in various setups, such as optical systems [80–83], electrical circuits [84–86], synthetic mechanical metamaterials [87–89], and ultracold atoms in synthetic momentum lattices [55–57,90,91]. In the above-mentioned systems, nonreciprocal hopping schemes can be tuned in the two-mode case, which corresponds to the nonreciprocal TLS. For instance, in the experimental implementation of ultracold atoms in synthetic momentum lattices, the discrete momentum states of ultracold atoms are coupled by using multiphoton processes [55–57,90,91]. In this system, the laser-induced hopping can be controlled independently by adjusting the corresponding lasers and the atomic interactions can be tuned by adjusting the  $s$ -wave scattering length. In particular, the influence of momentum-space interactions on population dynamics of ultracold atoms in a coupled double well has been explored [55]. Since the results of this work provide useful information for understanding the dynamics of non-Hermitian physics, we hope that our studies will stimulate experiments in this direction.

In summary, we have utilized the multiple-passage LZSM scheme of a self-interacting nonreciprocal TLS to explore quantum interference in non-Hermitian systems. We focused on the influence of the appearance of EPs on quantum interference behavior. In the absence of nonlinear interaction, our findings indicate that quantum interference is maintained in the weak nonreciprocal regime, whereas it is completely suppressed in the strong nonreciprocal regime due to  $\mathcal{PT}$ -symmetry breaking. It is worth emphasizing that the interesting phenomenon of the disappearance of the fringe does not occur in the reciprocal case (i.e.,  $\delta = 0$ ). In the framework of the RWA, we provided a complete theoretical explanation. The appearance of EPs can be changed by both nonreciprocity and nonlinearity parameters. The competition between nonreciprocity and nonlinearity yields a rich variety of quantum interference. Explicit phase diagrams were obtained, showing the phase of the breakdown of quantum interference by a strong nonreciprocity, the self-trapping phase, and the phase in which quantum interference is maintained, for a large range of nonreciprocity and nonlinearity parameters. Our theoretical studies extend the understanding of novel dynamics of non-Hermitian systems and may provide a theoretical perspective for the manipulation of quantum states in non-Hermitian systems both theoretically and experimentally.

## ACKNOWLEDGMENTS

We are grateful to Prof. Jie Liu for his valuable suggestions and discussions. This work was supported by the National Natural Science Foundation of China (Contracts No.

12005173 and No. 12365004) and the Natural Science Foundation of Gansu Province (Contract No. 20JR10RA082).

### APPENDIX A: DERIVATION OF THE ANALYTIC EXPRESSION UNDER THE FRAMEWORK OF THE RWA

It is useful to make use of a suitable RWA to analyze the above dynamics under high-frequency driving, i.e.,  $\omega \gg \nu$ . First we consider a Hamiltonian in Eq. (1) describing a linear system and make a transformation to a rotating frame with the operator  $U$ :

$$\hat{U}(t) = \exp \left[ -\frac{i}{2} \left( \frac{A}{w} \sin \omega t \right) \hat{\sigma}_z \right]. \quad (\text{A1})$$

This operator connects the wave function in the reference frame  $\begin{pmatrix} a \\ b \end{pmatrix}$  to the wave function in the rotating frame  $\begin{pmatrix} a' \\ b' \end{pmatrix}$ ,

$$\begin{pmatrix} a \\ b \end{pmatrix} = \hat{U}(t) \begin{pmatrix} a' \\ b' \end{pmatrix}. \quad (\text{A2})$$

Then the dimensionless Schrödinger equation in the rotating frame can be expressed as

$$i \frac{d}{dt} \begin{pmatrix} a' \\ b' \end{pmatrix} = \hat{H}'(t) \begin{pmatrix} a' \\ b' \end{pmatrix}, \quad (\text{A3})$$

where

$$\begin{aligned} \hat{H}'(t) &= \hat{U}(t)^\dagger \hat{H}(t) \hat{U}(t) - i \hat{U}(t)^\dagger \frac{d\hat{U}(t)}{dt} \\ &= \frac{\nu}{2} \begin{pmatrix} 0 & e^{i(A/\omega \sin \omega t)} \\ (1-\delta)e^{-i(A/\omega \sin \omega t)} & 0 \end{pmatrix}. \end{aligned} \quad (\text{A4})$$

We now make use of the Jacobi-Anger relation

$$e^{i(A/\omega) \sin \gamma} = \sum_{n=-\infty}^{\infty} J_n \left( \frac{A}{\omega} \right) e^{iny}, \quad (\text{A5})$$

where  $J_n(A/\omega)$  is the  $n$ th-order Bessel function of the first kind. So we obtain the final expression of the new Hamiltonian

$$H' = \frac{\nu}{2} \begin{pmatrix} 0 & \sum_{n=-\infty}^{\infty} J_n \left( \frac{A}{w} \right) e^{in\omega t} \\ \sum_{n=-\infty}^{\infty} (1-\delta) J_n \left( \frac{A}{w} \right) e^{-in\omega t} & 0 \end{pmatrix}. \quad (\text{A6})$$

For the high-frequency case, the fact that the contribution of higher-order Bessel functions is small enough means that we can neglect it. Therefore, we further simplify the Hamiltonian by keeping only the dominant term (i.e., the zeroth-order Bessel function)

$$H' = \frac{\nu}{2} \begin{pmatrix} 0 & J_0 \left( \frac{A}{w} \right) \\ (1-\delta) J_0 \left( \frac{A}{w} \right) & 0 \end{pmatrix}. \quad (\text{A7})$$

Substituting Eq. (A7) into the Schrödinger equation and simultaneously considering the initial condition  $(a(t=0), b(t=0))^T = (0, 1)^T$ , we readily obtain

$$a(t) = \frac{i \sin(B\sqrt{1-\delta}t)}{\sqrt{1-\delta}}, \quad (\text{A8a})$$

$$b(t) = \cos(B\sqrt{1-\delta}t), \quad (\text{A8b})$$

where  $B = \frac{\nu}{2} J_0 \left( \frac{A}{\omega} \right)$ . Then the quantum interference fringe patterns can be obtained by recording the occupancy probability  $P_a$  [defined in Eq. (4)] as

$$P_a = \begin{cases} \frac{1}{\delta + (1-\delta) \csc^2(B\sqrt{1-\delta}t)}, & \delta < 1 \\ \frac{1}{\delta + (\delta-1) \csc^2[B\sqrt{\delta-1}t]}, & \delta > 1. \end{cases} \quad (\text{A9})$$

Concerning the initial condition  $(a(t=0), b(t=0))^T = (1, 0)^T$ , we readily obtain

$$a(t) = \cos(B\sqrt{1-\delta}t), \quad (\text{A10a})$$

$$b(t) = i\sqrt{1-\delta} \sin(B\sqrt{1-\delta}t). \quad (\text{A10b})$$

Then the quantum interference fringe patterns can be obtained by recording the occupancy probability  $P_b$  [defined in Eq. (4)] as

$$P_b = \begin{cases} \frac{\delta-1}{\delta} \left( 1 - \frac{2}{2-\delta+\delta \cos(2B\sqrt{1-\delta}t)} \right), & \delta < 1 \\ \frac{\delta-1}{\delta} \left( 1 - \frac{2}{2-\delta+\delta \cosh(2B\sqrt{\delta-1}t)} \right), & \delta > 1. \end{cases} \quad (\text{A11})$$

From the above explicit expressions, we see that  $a(t)$  and  $b(t)$  vary with respect to time periodically in the weak nonreciprocal regime. They share a common period

$$T = \frac{2\pi}{\sqrt{1-\delta} \nu |J_0 \left( \frac{A}{\omega} \right)|}. \quad (\text{A12})$$

In the strong nonreciprocal regime, we can obtain, through enough LZSM processes, the values depending solely on the nonreciprocity parameter in the forms of  $P_a = 1/\delta$  and  $P_b = (\delta-1)/\delta$ .

### APPENDIX B: DYNAMICAL BEHAVIOR OF THE UNNORMALIZED AMPLITUDE OF A WAVE FUNCTION

The unnormalized amplitude  $P'_a \equiv |a(t)|^2$  for the system initially found in the upper energy level, i.e.,  $(a(t=0), b(t=0))^T = (0, 1)^T$ , can be readily obtained from Eq. (A8a) as

$$P'_a = \frac{\sin^2(B\sqrt{1-\delta}t)}{1-\delta} \quad (\delta < 1), \quad (\text{B1a})$$

$$P'_a = \frac{\sinh^2(B\sqrt{\delta-1}t)}{\delta-1} \quad (\delta > 1). \quad (\text{B1b})$$

The unnormalized amplitude  $P'_b \equiv |b(t)|^2$  for the system, initially found in the lower energy level, i.e.,  $(a(t=0), b(t=0))^T = (1, 0)^T$ , can be readily obtained from Eq. (A10b) as

$$P'_b = (1-\delta) \sin^2(B\sqrt{1-\delta}t) \quad (\delta < 1), \quad (\text{B2a})$$

$$P'_b = (\delta-1) \sinh^2(B\sqrt{\delta-1}t) \quad (\delta > 1). \quad (\text{B2b})$$

In Fig. 8 we present the nonreciprocal time-domain unnormalized amplitudes of wave function  $P'_a$  and  $P'_b$  obtained by directly integrating the time-dependent nonlinear Schrödinger equation and compare them with the above analytical formula calculated from the RWA, which shows they match each other well. From the expressions (B1) and (B2), one can clearly see that in the weak nonreciprocal regime, the unnormalized amplitudes of the wave function  $P'_a$  and  $P'_b$  oscillate

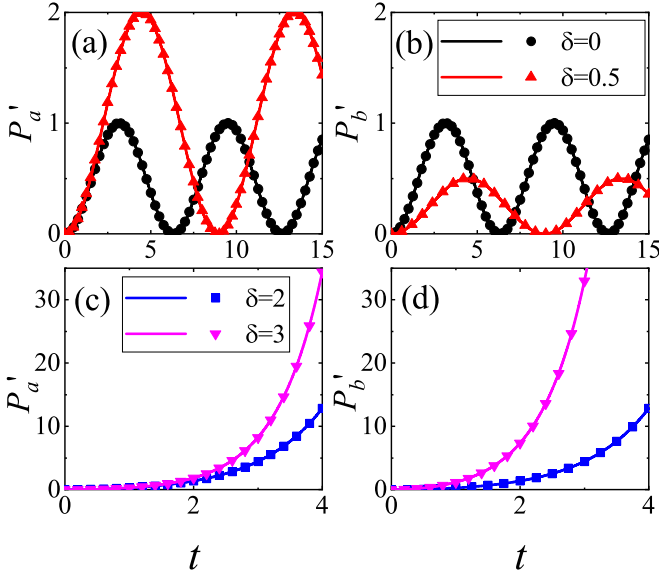


FIG. 8. Dynamical behavior of unnormalized amplitudes of wave function  $P'_a$  and  $P'_b$  obtained by directly integrating the time-dependent nonlinear Schrödinger equation (circles) and the theoretical results obtained using the expressions (B1) and (B2) (solid lines) for (a) and (b) the weak nonreciprocal regime, i.e.,  $\delta < 1$ , and (c) and (d) the strong nonreciprocal regime, i.e.,  $\delta > 1$ .

periodically with amplitudes  $1/(1-\delta)$  and  $1-\delta$ , respectively. In the strong nonreciprocal regime, both  $P'_a$  and  $P'_b$  rapidly increase with time evolution.

#### APPENDIX C: VALIDITY OF THE ANALYTICAL FORMULA UNDER HIGH-FREQUENCY APPROXIMATION

The analytical formulas are obtained from the framework of the RWA and by considering the high-frequency approximation that the present paper focuses on. To demonstrate at what frequency values the dynamics starts to deviate from the high-frequency limit, we introduce the two quantities

$$\Delta_a \equiv |P_a^{\text{num}} - P_a^{\text{ana}}|, \quad \Delta_b \equiv |P_b^{\text{num}} - P_b^{\text{ana}}|, \quad (\text{C1})$$

where  $P_a^{\text{num}}$  and  $P_b^{\text{num}}$  represent the numerical results obtained by directly integrating the time-dependent nonlinear Schrödinger equation and  $P_a^{\text{ana}}$  and  $P_b^{\text{ana}}$  represent the analytical results using expressions (5) and (6). These two quantities can reflect at what frequency values the dynamics starts to deviate from the high-frequency limit.

The results are shown in Fig. 9. In the strong nonreciprocal regime ( $\delta > 1$ ), it is interesting to show that both quantities  $\Delta_a$  and  $\Delta_b$  are approximately zero for  $\omega$  ranges from the low-frequency case to the high-frequency case. In the weak nonreciprocal regime ( $\delta < 1$ ), both quantities  $\Delta_a$  and  $\Delta_b$  exhibit significant fluctuations for the low frequency case, whereas they are indeed approximately zero for the high frequency case. In this regime, the window of frequency values for the dynamics starts to deviate from the high-frequency limit, becoming larger as  $\delta$  increases. The results in Fig. 9

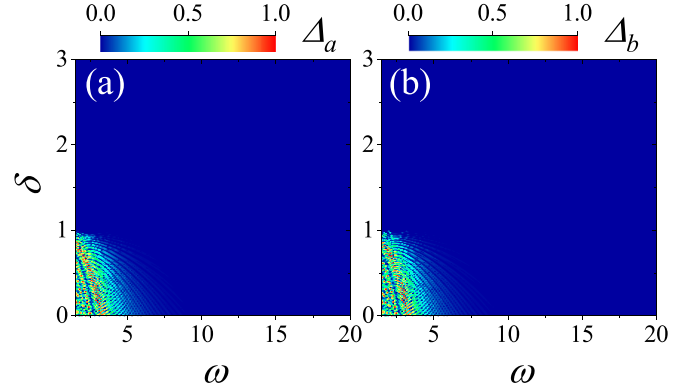


FIG. 9. Comparison of numerical results obtained by directly integrating the time-dependent nonlinear Schrödinger equation and analytical results using the expressions (5) and (6). Here the results are obtained by recording the final values during 100 periods of the LZSM process, i.e.,  $t = 10\pi$  for  $A = 3$ .

further strengthen the validity of the analytical formula under high-frequency approximation.

#### APPENDIX D: NUMERICAL RESULTS OF NONRECIPROCAL QUANTUM INTERFERENCE IN THE LARGE RANGE OF DRIVING FREQUENCY

The main results in the previous text focus on the high-frequency driving case, in the absence of nonlinear self-interaction, where we find that interference is completely suppressed in a strong nonreciprocal regime. To inspect whether the interesting phenomenon also exists in the case of low-frequency driving, we numerically solve the Schrödinger equation within the large range of driving frequency. Figures 10(a) and 10(b) depict the numerical results of quantum interference patterns as a function of the nonreciprocity parameter  $\delta$  and the driving amplitude  $\omega$  for the system that is initially found in the upper and lower energy levels, respec-

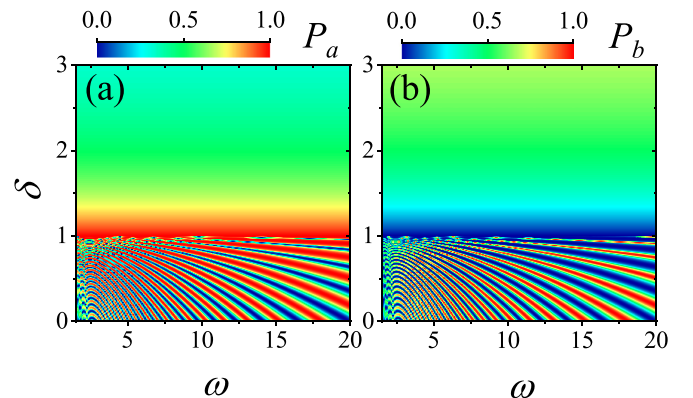


FIG. 10. Numerical results of nonreciprocal quantum interference patterns in the large range of driving frequency  $\omega$ . Level occupation probabilities (a)  $P_a$  and (b)  $P_b$  for the system are initially found in the upper and lower energy levels, respectively. Here the quantum interference patterns are obtained by recording the final occupancy probability  $P_a$  (or  $P_b$ ) during 100 periods of the LZSM process for  $A = 3$ .

tively. The numerical results show that the interference fringes are conspicuously present in weak nonreciprocal regime (i.e.,  $\delta < 1$ ), while the interference is completely suppressed in

strong nonreciprocal regime (i.e.,  $\delta > 1$ ). These results seem to clearly reveal that the interesting phenomenon of interference suppression is due to  $\mathcal{PT}$ -symmetry breaking.

- 
- [1] L. D. Landau, *Phys. Z. Sowjetunion* **2**, 46 (1932).
- [2] G. Zener, *Proc. R. Soc. London Ser. A* **137**, 696 (1932).
- [3] E. C. G. Stückelberg, *Helv. Phys. Acta* **5**, 369 (1932).
- [4] L. D. Landau, *Phys. Z. Sowjetunion* **1**, 88 (1932).
- [5] S.-C. Li, L.-B. Fu, and J. Liu, *Phys. Rev. A* **98**, 013601 (2018).
- [6] S. N. Shevchenko, S. Ashhab, and F. Nori, *Phys. Rep.* **492**, 1 (2010).
- [7] O. V. Ivakhnenko, S. N. Shevchenko, and F. Nori, *Phys. Rep.* **995**, 1 (2023).
- [8] M. Mark, T. Kraemer, P. Waldburger, J. Herbig, C. Chin, H.-C. Nägerl, and R. Grimm, *Phys. Rev. Lett.* **99**, 113201 (2007).
- [9] S. Kling, T. Salger, C. Grossert, and M. Weitz, *Phys. Rev. Lett.* **105**, 215301 (2010).
- [10] G. D. Fuchs, G. Burkard, P. V. Klimov, and D. D. Awschalom, *Nat. Phys.* **7**, 789 (2011).
- [11] G. D. Fuchs, V. V. Dobrovitski, D. M. Toyli, F. J. Heremans, and D. D. Awschalom, *Science* **326**, 1520 (2009).
- [12] M. B. Kenmoe and L. C. Fai, *Phys. Rev. B* **94**, 125101 (2016).
- [13] J.-N. Zhang, C.-P. Sun, S. Yi, and F. Nori, *Phys. Rev. A* **83**, 033614 (2011).
- [14] C. M. Bender and S. Boettcher, *Phys. Rev. Lett.* **80**, 5243 (1998).
- [15] V. V. Konotop, J. Yang, and D. A. Zezyulin, *Rev. Mod. Phys.* **88**, 035002 (2016).
- [16] L. Feng, R. El-Ganainy, and L. Ge, *Nat. Photon.* **11**, 752 (2017).
- [17] M.-A. Miri and A. Alù, *Science* **363**, eaar7709 (2019).
- [18] R. El-Ganainy, K. G. Makris, M. Khajavikhan, Z. H. Musslimani, S. Rotter, and D. N. Christodoulides, *Nat. Phys.* **14**, 11 (2018).
- [19] R. Bouganne, M. Bosch Aguilera, A. Ghermaoui, J. Beugnon, and F. Gerbier, *Nat. Phys.* **16**, 21 (2020).
- [20] Y. Ashida, Z. Gong, and M. Ueda, *Adv. Phys.* **69**, 249 (2020).
- [21] E. J. Bergholtz, J. C. Budich, and F. K. Kunst, *Rev. Mod. Phys.* **93**, 015005 (2021).
- [22] W.-Y. Wang, B. Sun, and J. Liu, *Phys. Rev. A* **106**, 063708 (2022).
- [23] X. Wang, H. D. Liu, and L. B. Fu, *New J. Phys.* **25**, 043032 (2023).
- [24] C. M. Bender, *Rep. Prog. Phys.* **70**, 947 (2007).
- [25] A. Mostafazadeh, *J. Math. Phys.* **43**, 205 (2002).
- [26] A. Mostafazadeh, *J. Phys. A: Math. Gen.* **36**, 7081 (2003).
- [27] T. Helbig, T. Hofmann, S. Imhof, M. Abdelghany, T. Kiessling, L. W. Molenkamp, C. H. Lee, A. Szameit, M. Greiter, and R. Thomale, *Nat. Phys.* **16**, 747 (2020).
- [28] L. M. Sieberer, S. D. Huber, E. Altman, and S. Diehl, *Phys. Rev. Lett.* **110**, 195301 (2013).
- [29] A. Metelmann and A. A. Clerk, *Phys. Rev. X* **5**, 021025 (2015).
- [30] R. Hanai, A. Edelman, Y. Ohashi, and P. B. Littlewood, *Phys. Rev. Lett.* **122**, 185301 (2019).
- [31] M. Fruchart, R. Hanai, P. B. Littlewood, and V. Vitelli, *Nature (London)* **592**, 363 (2021).
- [32] R. Hanai and P. B. Littlewood, *Phys. Rev. Res.* **2**, 033018 (2020).
- [33] D. L. Sounas and A. Alù, *Nat. Photon.* **11**, 774 (2017).
- [34] Y. Castin and R. Dum, *Phys. Rev. Lett.* **79**, 3553 (1997).
- [35] Y. Castin and R. Dum, *Phys. Rev. A* **57**, 3008 (1998).
- [36] J. Liu, C. Zhang, M. G. Raizen, and Q. Niu, *Phys. Rev. A* **73**, 013601 (2006).
- [37] W. P. Su, J. R. Schrieffer, and A. J. Heeger, *Phys. Rev. B* **22**, 2099 (1980).
- [38] Z. Wang, Y. Chong, J. D. Joannopoulos, and M. Soljačić, *Nature (London)* **461**, 772 (2009).
- [39] X.-L. Qi and S.-C. Zhang, *Phys. Today* **63** (1), 33 (2010).
- [40] C. Coulais, D. Sounas, and A. Alù, *Nature (London)* **542**, 461 (2017).
- [41] L. Feng, Y.-L. Xu, W. S. Fegadolli, M.-H. Lu, J. E. B. Oliveira, V. R. Almeida, Y.-F. Chen, and A. Scherer, *Nat. Mater.* **12**, 108 (2013).
- [42] K. Stannigel, P. Komar, S. J. M. Habraken, S. D. Bennett, M. D. Lukin, P. Zoller, and P. Rabl, *Phys. Rev. Lett.* **109**, 013603 (2012).
- [43] J. Kim, M. C. Kuzyk, K. Han, H. Wang, and G. Bahl, *Nat. Phys.* **11**, 275 (2015).
- [44] S. Barzanjeh, M. Aquilina, and A. Xuereb, *Phys. Rev. Lett.* **120**, 060601 (2018).
- [45] H. Li, T. Kottos, and B. Shapiro, *Phys. Rev. Appl.* **9**, 044031 (2018).
- [46] J. Dalibard, Y. Castin, and K. Mølmer, *Phys. Rev. Lett.* **68**, 580 (1992).
- [47] K. Mølmer, Y. Castin, and J. Dalibard, *J. Opt. Soc. Am. B* **10**, 524 (1993).
- [48] R. Dum, P. Zoller, and H. Ritsch, *Phys. Rev. A* **45**, 4879 (1992).
- [49] M. B. Plenio and P. L. Knight, *Rev. Mod. Phys.* **70**, 101 (1998).
- [50] A. J. Daley, *Adv. Phys.* **63**, 77 (2014).
- [51] L. Xiao, T. Deng, K. Wang, G. Zhu, Z. Wang, W. Yi, and P. Xue, *Nat. Phys.* **16**, 761 (2020).
- [52] Z. Gong, Y. Ashida, K. Kawabata, K. Takasan, S. Higashikawa, and M. Ueda, *Phys. Rev. X* **8**, 031079 (2018).
- [53] D.-W. Zhang, Y.-Q. Zhu, Y. X. Zhao, H. Yan, and S.-L. Zhu, *Adv. Phys.* **67**, 253 (2018).
- [54] H. Carmichael, *An Open Systems Approach to Quantum Optics, Lecture Notes in Physics Monographs*, Vol. 18 (Springer, Berlin, 1993).
- [55] F. A. An, E. J. Meier, J. Ang'ong'a, and B. Gadway, *Phys. Rev. Lett.* **120**, 040407 (2018).
- [56] W. Gou, T. Chen, D. Xie, T. Xiao, T.-S. Deng, B. Gadway, W. Yi, and B. Yan, *Phys. Rev. Lett.* **124**, 070402 (2020).
- [57] Q. Liang, D. Xie, Z. Dong, H. Li, H. Li, B. Gadway, W. Yi, and B. Yan, *Phys. Rev. Lett.* **129**, 070401 (2022).
- [58] B. T. Torosov and N. V. Vitanov, *Phys. Rev. A* **96**, 013845 (2017).
- [59] E. M. Graefe and H. J. Korsch, *Czech. J. Phys.* **56**, 1007 (2006).
- [60] S. A. Reyes, F. A. Olivares, and L. Morales-Molina, *J. Phys. A: Math. Theor.* **45**, 444027 (2012).
- [61] Y. Lumer, Y. Plotnik, M. C. Rechtsman, and M. Segev, *Phys. Rev. Lett.* **111**, 263901 (2013).
- [62] P. I. Kam Wa, J. E. Sitch, N. J. Mason, J. S. Roberts, and P. N. Robson, *Electron. Lett.* **21**, 26 (1985).

- [63] U. Das, Y. Chen, and P. Bhattacharya, *Appl. Phys. Lett.* **51**, 1679 (1987).
- [64] H. Ramezani, T. Kottos, R. El-Ganainy, and D. N. Christodoulides, *Phys. Rev. A* **82**, 043803 (2010).
- [65] P. Aleahmad, M. Khajavikhan, D. Christodoulides, and P. LiKamWa, *Sci. Rep.* **7**, 2129 (2017).
- [66] S. Longhi, *Opt. Lett.* **43**, 5371 (2018).
- [67] S. Longhi, *Opt. Lett.* **43**, 2929 (2018).
- [68] F. Grossmann, T. Dittrich, P. Jung, and P. Hänggi, *Phys. Rev. Lett.* **67**, 516 (1991).
- [69] F. Großmann and P. Hänggi, *Europhys. Lett.* **18**, 571 (1992).
- [70] S. Ashhab, J. R. Johansson, A. M. Zagoskin, and F. Nori, *Phys. Rev. A* **75**, 063414 (2007).
- [71] J. Liu, L. Fu, B.-Y. Ou, S.-G. Chen, D.-I. Choi, B. Wu, and Q. Niu, *Phys. Rev. A* **66**, 023404 (2002).
- [72] G.-F. Wang, L.-B. Fu, and J. Liu, *Phys. Rev. A* **73**, 013619 (2006).
- [73] D.-F. Ye, L.-B. Fu, and J. Liu, *Phys. Rev. A* **77**, 013402 (2008).
- [74] J. Liu, L.-B. Fu, B. Liu, and B. Wu, *New J. Phys.* **10**, 123018 (2008).
- [75] S.-C. Li, L.-B. Fu, W.-S. Duan, and J. Liu, *Phys. Rev. A* **78**, 063621 (2008).
- [76] J. Liu, B. Liu, and L.-B. Fu, *Phys. Rev. A* **78**, 013618 (2008).
- [77] F. Q. Dou, L. B. Fu, and J. Liu, *Phys. Rev. A* **89**, 012123 (2014).
- [78] F.-Q. Dou, H. Cao, J. Liu, and L.-B. Fu, *Phys. Rev. A* **93**, 043419 (2016).
- [79] F.-Q. Dou, J. Liu, and L.-B. Fu, *Phys. Rev. A* **98**, 022102 (2018).
- [80] B. Peng, Ş. K. Özdemir, F. Lei, F. Monifi, M. Gianfreda, G. L. Long, S. Fan, F. Nori, C. M. Bender, and L. Yang, *Nat. Phys.* **10**, 394 (2014).
- [81] F. Ruesink, M.-A. Miri, A. Alù, and E. Verhagen, *Nat. Commun.* **7**, 13662 (2016).
- [82] K. Fang, J. Luo, A. Metelmann, M. H. Matheny, F. Marquardt, A. A. Clerk, and O. Painter, *Nat. Phys.* **13**, 465 (2017).
- [83] S. Weidemann, M. Kremer, T. Helbig, T. Hofmann, A. Stegmaier, M. Greiter, R. Thomale, and A. Szameit, *Science* **368**, 311 (2020).
- [84] M. Ezawa, *Phys. Rev. B* **99**, 121411(R) (2019).
- [85] M. Ezawa, *Phys. Rev. B* **100**, 165419 (2019).
- [86] S. Liu, R. Shao, S. Ma, L. Zhang, O. You, H. Wu, Y. J. Xiang, T. J. Cui, and S. Zhang, *Research* **2021**, 5608038 (2021).
- [87] R. Anandwade, Y. Singhal, S. N. M. Paladugu, E. Martello, M. Castle, S. Agrawal, E. Carlson, C. Battle-McDonald, T. Ozawa, H. M. Price, and B. Gadway, *Phys. Rev. A* **108**, 012221 (2023).
- [88] Y. Singhal, E. Martello, S. Agrawal, T. Ozawa, H. Price, and B. Gadway, *Phys. Rev. Res.* **5**, L032026 (2023).
- [89] E. Martello, Y. Singhal, B. Gadway, T. Ozawa, and H. M. Price, *Phys. Rev. E* **107**, 064211 (2023).
- [90] F. A. An, B. Sundar, J. Hou, X.-W. Luo, E. J. Meier, C. Zhang, K. R. A. Hazzard, and B. Gadway, *Phys. Rev. Lett.* **127**, 130401 (2021).
- [91] T. Yuan, C. Zeng, Y.-Y. Mao, F.-F. Wu, Y.-J. Xie, W.-Z. Zhang, H.-N. Dai, Y.-A. Chen, and J.-W. Pan, *Phys. Rev. Res.* **5**, L032005 (2023).